Supporting Information

Interface-Driven Construction of Three-Dimensional Silver-Carbon Aerogels via Microwave Radiation for Thermal Regulation

Jiaheng Hu[a,b#], Jun Zhu[a,c#], Yan Hu[a,c#*], Jialu Yang[d], Yinghua Ye[a,c], Ruiqi Shen[a,c]

a *School of Chemistry and Chemical Engineering, Nanjing University of Science and Technology, Nanjing 210094, China*

b *Department of Mechanical and Energy Engineering, Southern University of Science and Technology, Shenzhen 518055, China*

c Micro-Nano Energetic Devices Key Laboratory of MIIT, Nanjing 210094, China

d Department of Electrical, Electronic and Computer Engineering, The University of Western Australia, 35 Stirling Highway, Crawley 6009, Australia

#These authors contributed equally to this work.

*** Corresponding author**:
Yan Hu
E-mail: huyan@njust.edu.cn
Full postal address: School of Chemistry and Chemical Engineering, Nanjing University of Science and Technology, Nanjing 210094, China
Telephone: +86-130-7349-3169

Experimental section

1.1. Materials

The raw materials for this experiment were graphene oxide (AR, Sigma-Aldrich), carbon nanotubes (AR, Tianjin Heowns), silver nitrate and 1-Butyl-3-methylimidazole tetrafluoroborate (AR, Shanghai Aladdin), sodium hydroxide (Shanghai Wokai Biotechnology Co., Ltd.), glutaraldehyde (Shanghai Myriad Biochemical Technology Co., Ltd.), Triton X-100 (AR, GLPBIO), ethanol (AR, Nanjing RongHua) and chitosan (AR, Sarn Chemical Technology (Shanghai) Co.)

1.2. Synthesis of SGC

The synthetic route of SGC is schematically shown in the design section. First, 0.1 g of graphene oxide (GO) was uniformly dispersed in ethanol solution (ethanol: water = 3:8) and 3 ml of [BMIM]BF_4 ionic liquid dilution was added for sonication. Next, 60 mg of carbon nanotubes (CNTs) and 2.8% of Triton X-100 solution were blended. The GO dispersion was mixed with the CNTs dispersion and 11 ml of 0.1 M silver nitrate solution was introduced. After waiting for the solution to be sonicated and dispersed, it was placed in a microwave reactor. 300 W, 400 W, and 500 W microwave power continued for 2, 1, and 2 min,

respectively. Finally, 400 W radiation lasting for 3 min was used as the end of the reaction. The residual solution was removed by washing. The silver-modified reduced graphene oxide /carbon nanotube composite powder was obtained by drying. The content of carbon nanotubes was added at 20, 40, 60, 80, and 100 mg and noted as GC1, GC2, GC3, GC4, and GC5, respectively, provided that other conditions remained unchanged. Further, the amount of silver nitrate was adjusted to 3, 7, 11, and 15 ml and was noted as SGC1, SGC2, SGC3, and SGC4, with GC3 as the research subject. Finally, the optimal ones were recorded as SGC for subsequent aerogel construction experiments. To compare the thermal effects of microwave irradiation versus conventional heating, the reaction mixture was placed in a hydrothermal reactor and reacted at 120°C in an oven for 6 hours using the GC3 synthesis route as the standard, labeled as C-GC.

1.3. Fabrication of SGCC composite aerogel/ITO thin film

In order to prepare chitosan composite carbon-based aerogel (SGCC) materials, we used a simple method of acid-base regulation [18]. First, 4 g of chitosan powder was put into 50.0 ml of 4% aqueous acetic acid solution and further stirred to dissolve it completely. SGC powder was added to 2 g of chitosan solution and 8 ml of deionized water. After ultrasonication for 30 minutes, 10% NaOH was sprayed on top of the solution. The manufactured hydrogel was left overnight and then removed for washing.

The hydrogels were soaked with 5% glutaraldehyde solution for 12 hours. After the complete removal of the solvent, the lyophilization operation is necessary to maintain the layered porous structure. At last, the surface of the aerogel has adhered with a layer of polyethylene terephthalate (PET) flexible film sputtered with transparent indium tin oxide (ITO) on outer side. The thin film thickness was 0.125 mm.

1.4. Characterization

In this experiment, diffraction angles ranging from 5° to 90° were used to analyze the crystal structure of the fabricated samples using an X-ray diffraction instrument (XRD, Rigaku SmartLab SE, Japan). The microscopic morphology of the carbon-based composites was observed by scanning electron microscopy (SEM, ZEISS Sigma 300, Germany) and transmission electron microscope (TEM, JEOL JEM 2100F, Japan). The element C, N, O, and Ag distribution was determined by the SEM and TEM with energy dispersive X-ray spectrometry. Raman spectra of samples irradiated at 532 nm with a Raman spectrometer (Horiba LabRAM HR Evolution, Japan) can indicate the degree of defects in carbon materials. An X-ray photoelectron spectrometer (XPS, Thermo Scientific K-Alpha, USA) was used to characterize the surface chemical properties. Infrared spectra of the samples were recorded by Fourier transform infrared (FT-IR) spectrometer (Nicolet iS50) equipped with an integrating sphere with

the wavenumber range from 7800 cm^{-1} to 400 cm^{-1}, which means that the wavelength ranges from 1.282 μm to 25 μm. At room temperature, mercury intrusion porosimetry (MIP) was conducted using a Micro AutoPore IV 9500 to measure porosity and pore size distribution. The compression properties of the aerogels were tested on a TY8000-A electronic universal testing machine. The thermal diffusivity coefficient was measured via laser thermal conductivity meter. The anisotropic thermal conductivity coefficient was obtained using the TPS2500S based on the hotdisk method. Thermal stability was measured with a thermalgravimetric analyzer (TA Q600, USA) under a nitrogen flow at a heating rate of 10 ℃·min^{-1}. The infrared images were taken with an infrared camera (Hr 300).

1.5. Calculation details

Molecular Dynamics Simulation：

The OPLS-AA force field [2] and Auxiliary Tools of Force Field（AuToFF）were used to parametrize all atoms of graphene and carbon nanotubes molecule, such as the bond parameters, angle parameters and the dihedral angles, and so on. The force field parameters of Ag atoms are referenced [3].

The adsorption behavior of Ag atoms at the graphene-carbon nanotube composite interface was simulated by molecular dynamics (MD) simulation.

First, a graphene and carbon nanotube composite substrate was constructed, that is, two interlaced carbon nanotubes were randomly added to the surface of graphene. Then, Ag atoms (2800) were randomly added to the graphene-carbon nanotube composite substrate to build an initial adsorption model.

The MD simulations were performed in the GROMACS 2021 software package[4-6] . The steepest descent method was applied to minimize the initial energy for each system with a force tolerance of 1 kJ (mol^{-1} nm^{-1}) and a maximum step size of 0.001 ps before MD calculations[7]. In all the three directions, periodic boundary conditions were imposed. Leapfrog algorithm was used to integrate the Newtonian equation of motion. The adsorption simulation was processed in an NVT ensemble and the simulation time is 20 ns.

In NVT simulation, the temperature was maintained by the V-rescale thermostat at 1000 K. The LINCS algorithm [8] was performed for constrain bond lengths of hydrogen atoms. The Particle-Mesh-Ewald (PME) with a fourth-order interpolation was used to evaluate the electrostatic interactions and whereas a cutoff of 1.0 nm was employed to calculate the short-range van der Waals interactions [9].

Density functional theory (DFT) calculations:

All density functional theory (DFT) calculations were performed using the Vienna Ab initio Simulation Package (VASP)[10,11]. Exchange–

correlation interactions were treated within the generalized gradient approximation (GGA) using the Perdew–Burke–Ernzerhof (PBE) functional [12], and the projector augmented-wave (PAW) method [13] described electron–ion interactions. A plane-wave cutoff energy of 500 eV was applied throughout, and dispersion forces were included via Grimme's DFT-D3 scheme with Becke–Johnson damping [14]. Electronic and ionic convergence thresholds of 1×10^{-5}eV and 0.02 eV $Å^{-1}$, respectively, were applied throughout.

First, defective graphene and defective carbon nanotube (CNT) models were fully relaxed (atomic positions and, where appropriate, the periodic cell parameter along the tube axis) using a 4×4×1 and 1×4×1 Monkhorst–Pack k-point mesh for the graphene and CNT models, respectively. For both systems a vacuum region exceeding 15 Å was introduced in the directions perpendicular to the periodic axis to avoid spurious image–image interactions. After geometry optimization of the bare defected substrates, adsorption models were constructed by placing a single Ag atom at the defect site; these slab+Ag structures were then re-optimized using the same computational parameters and k-point samplings. Subsequent single-point self-consistent calculations were performed on the relaxed geometries with the same cutoff, k-point grids and convergence criteria to obtain final energies and charge densities. Differential charge densities were obtained as $\Delta\rho=\rho_{total}-\rho_{substrate}-\rho_{Ag}$ and visualized as

isosurfaces to identify charge accumulation and depletion at the adsorption site. Bader charge analysis (using the grid-based algorithm) was carried out on the converged total charge density to quantify charge transfer between Ag and the defective substrates.

Adsorption energies (E_{ads}) are calculated using the following formula:

$$E_{ads} = E_{total} - E_{slab} - E_{adsorbent}$$

Where E_{total}, E_{slab}, and $E_{adsorbent}$ denote the DFT total energies of the slab + Ag system, the clean slab alone (with vacuum), and the isolated Ag molecule (in the same vacuum environment), respectively.

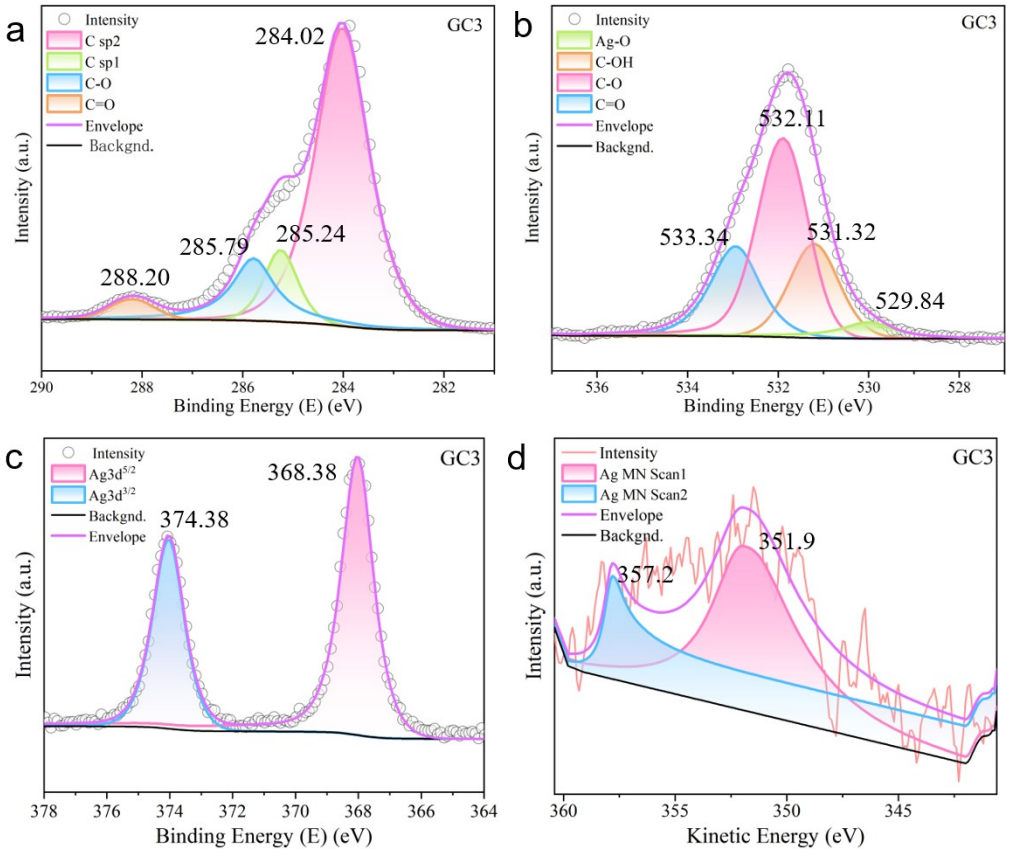

Fig. S1. XPS spectrum of (a) C 1s, (b) O 1s, (c) Ag 3d, and (d) Ag Auger peaks about GC3.

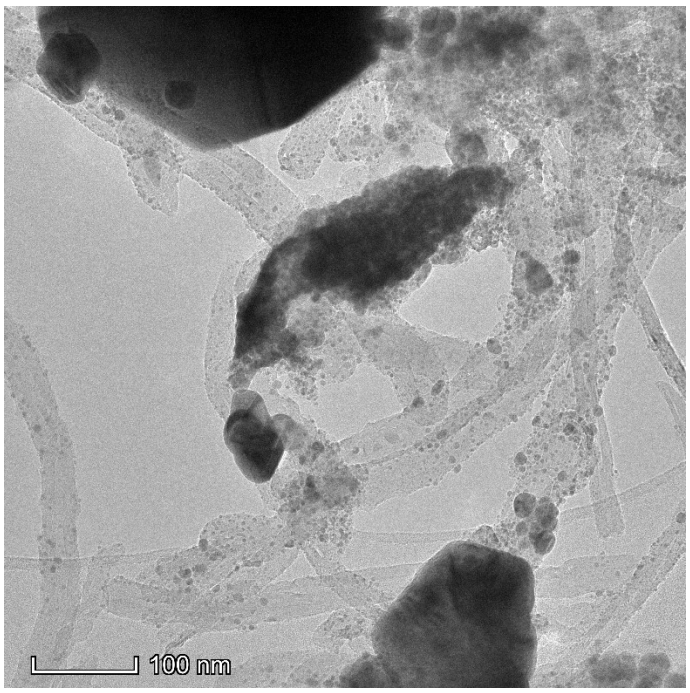

Fig. S2. TEM image of C-GC

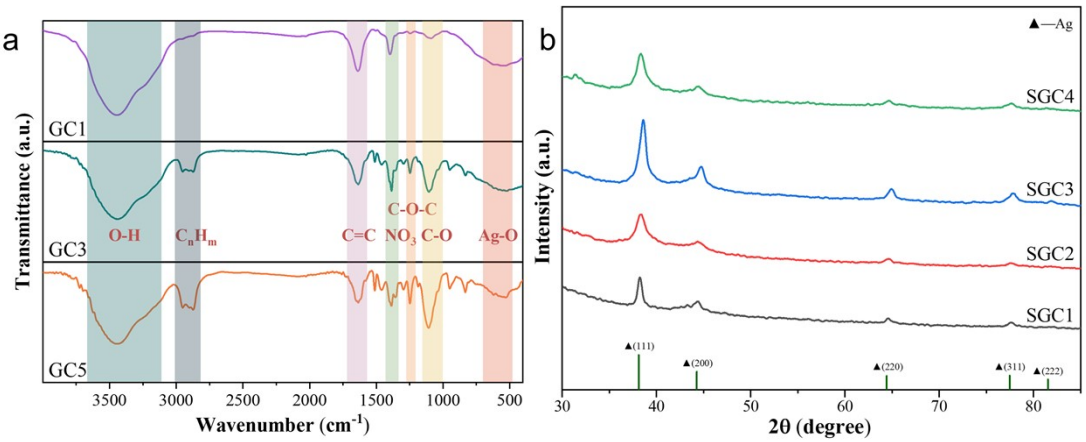

Fig. S3. (a) FT-IR spectra of GC1, GC3, GC5. (b) XRD patterns for different silver nitrate additions.

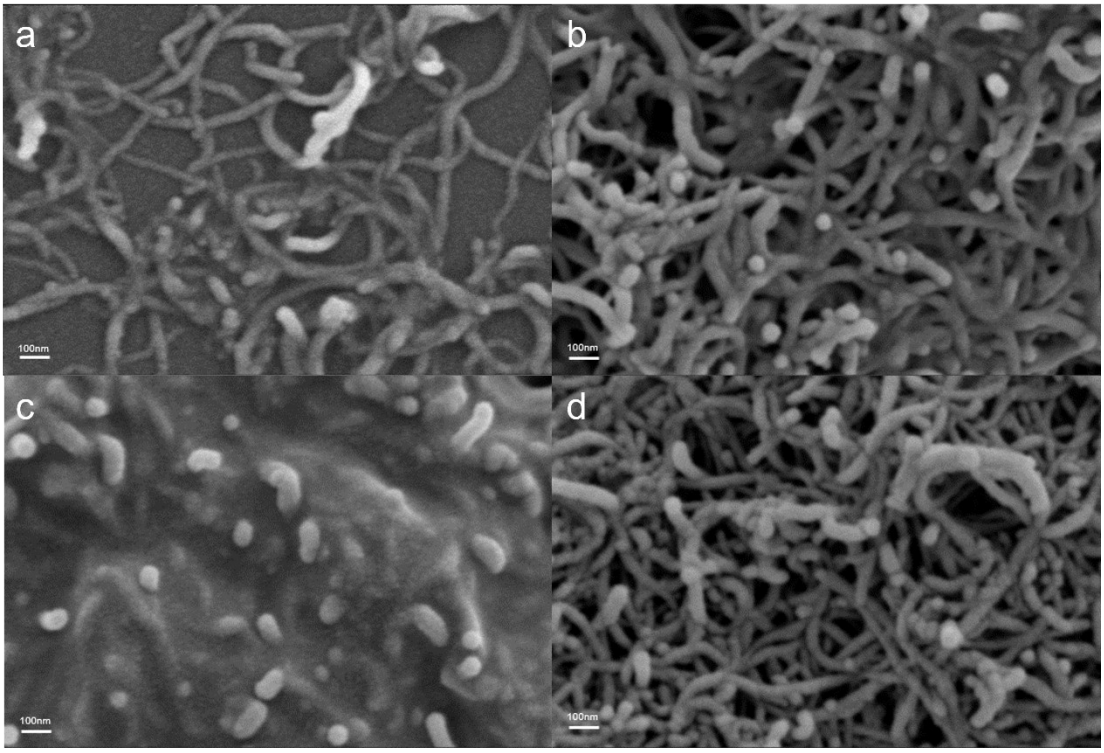

Fig. S4. SEM images of SGC1-4.

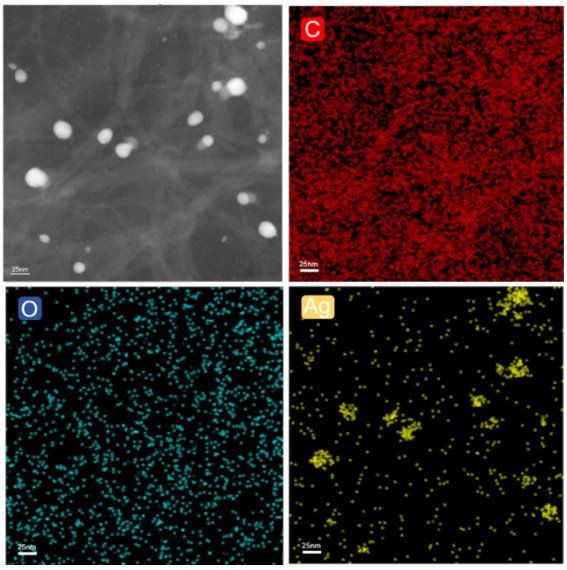

Fig. S5. EDS images of SGC3.

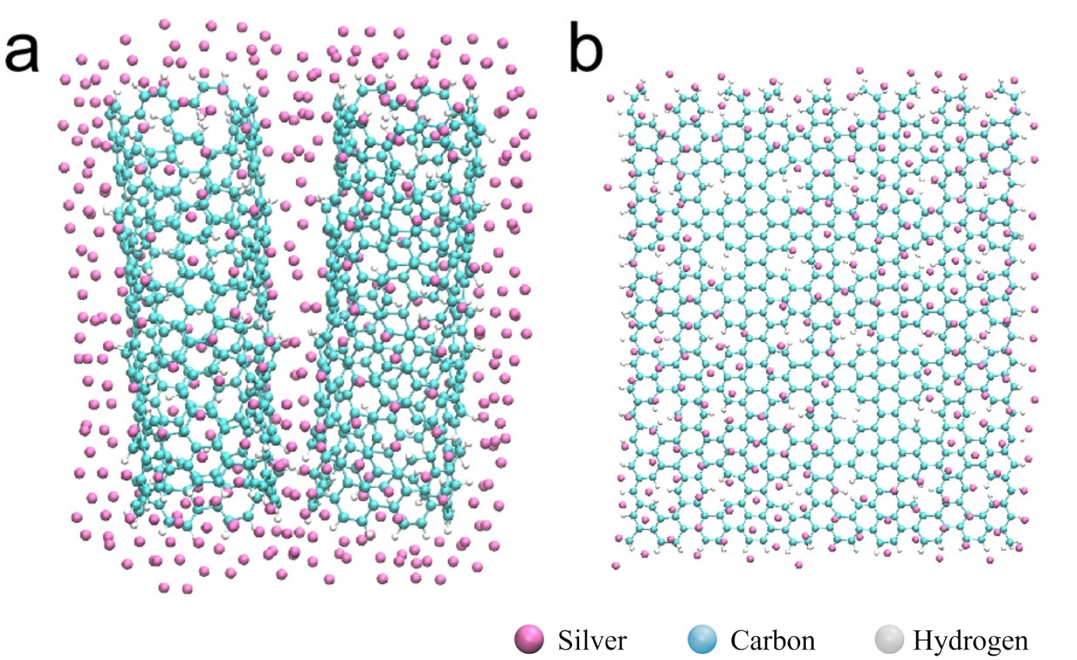

Fig. S6. (a) Local structure from dynamics simulation of Ag atom adsorption on carbon nanotubes. (b) Local structure from dynamics simulation of Ag atom adsorption on graphene.

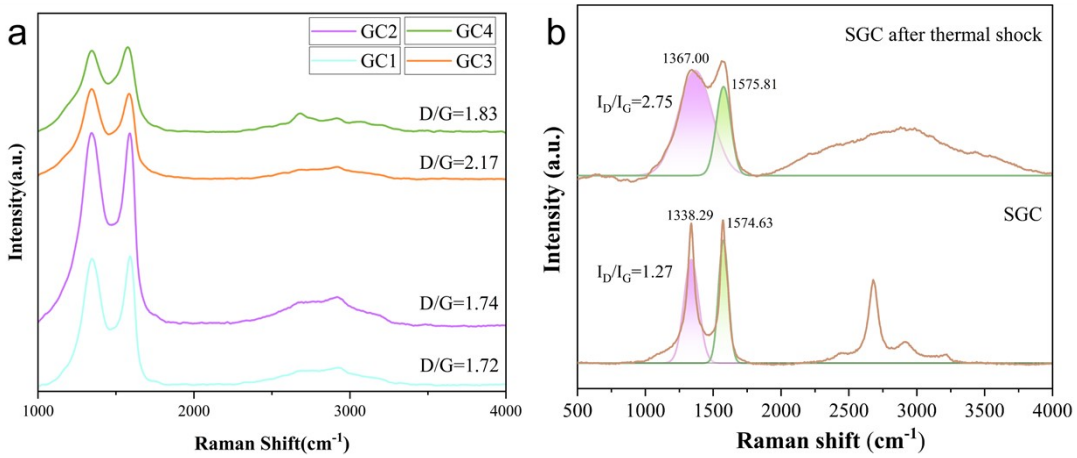

Fig. S7. (a) Raman spectrum of GC1, GC2, GC3, and GC4. (b) Raman spectrum of SGC and SGC after thermal shock.

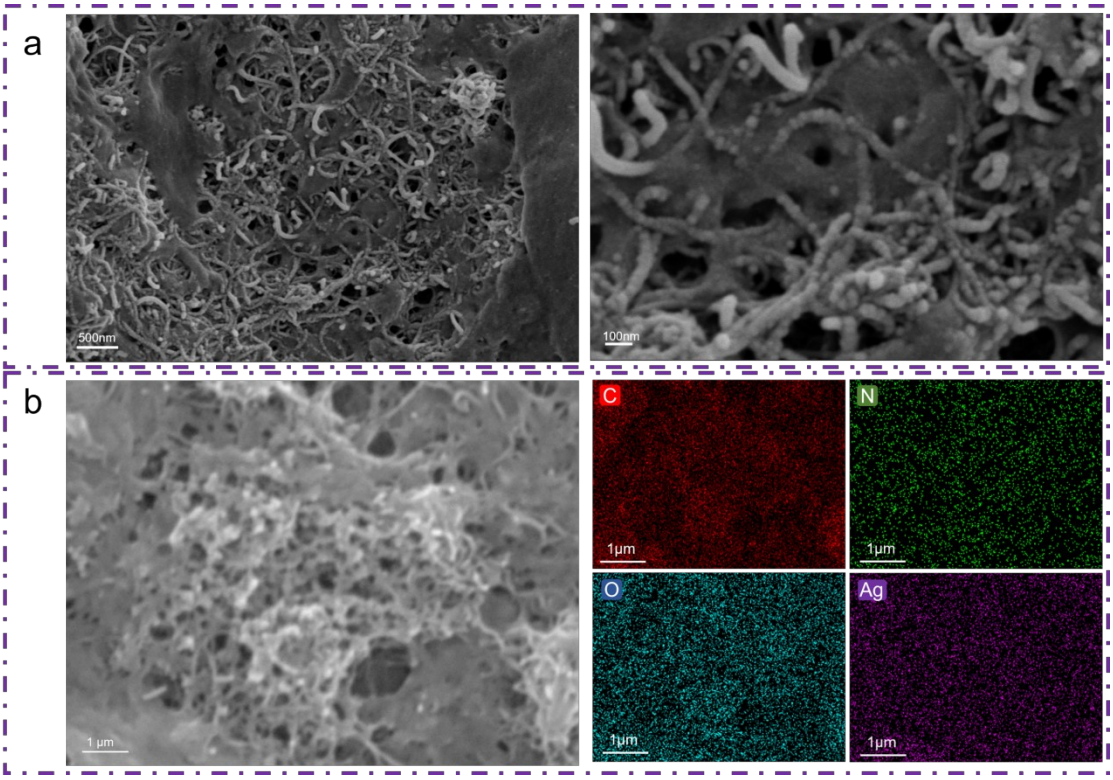

Fig. S8. (a) SEM images of SGCC. (b) EDS mapping of SGCC.

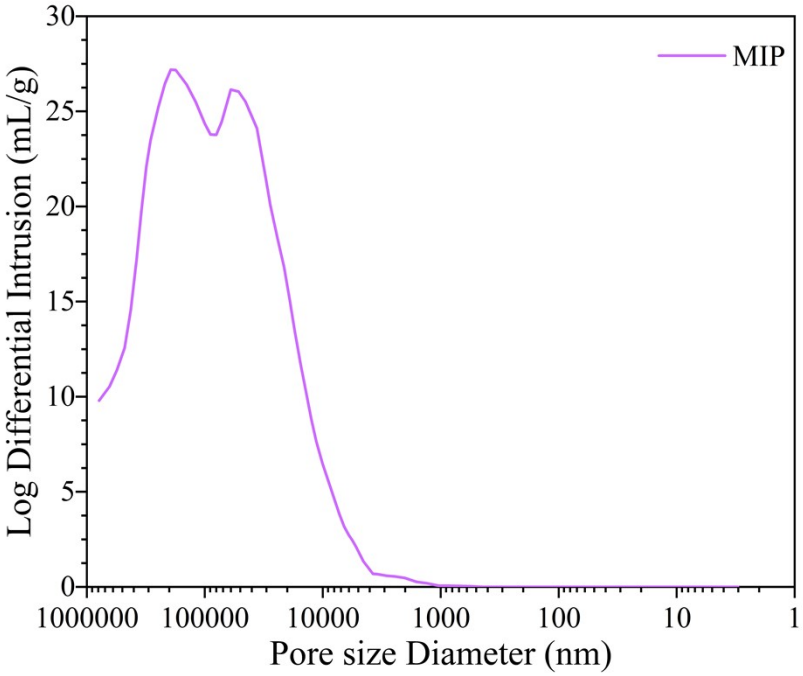

Fig. S9. Pore size distribution of SGCC.

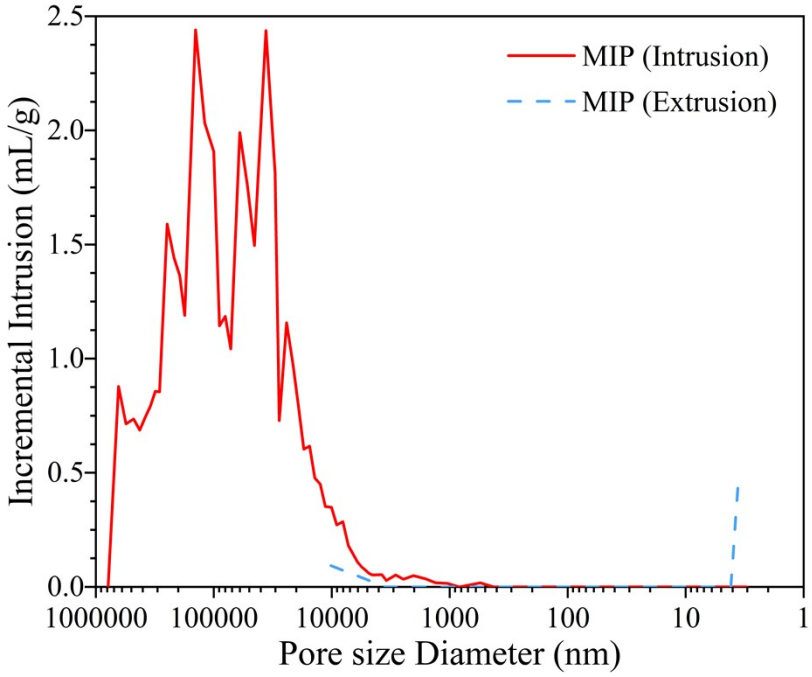

Fig. S10. Intrusion and extrusion curves of SGCC.

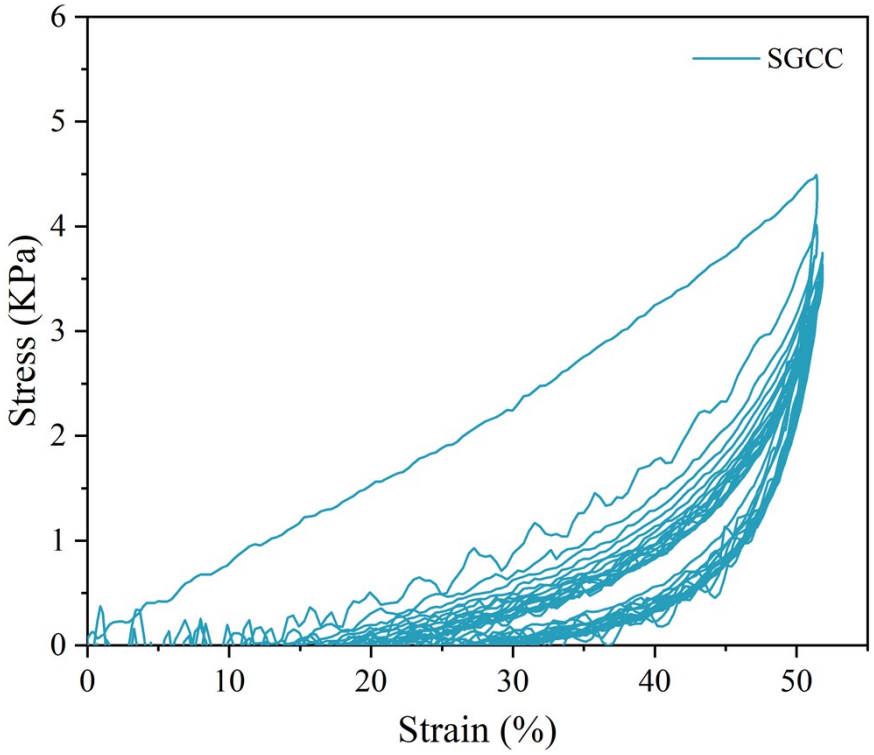

Fig. S11. Cyclic compressive stress–strain curves of the SGCC aerogel under 50% strain.

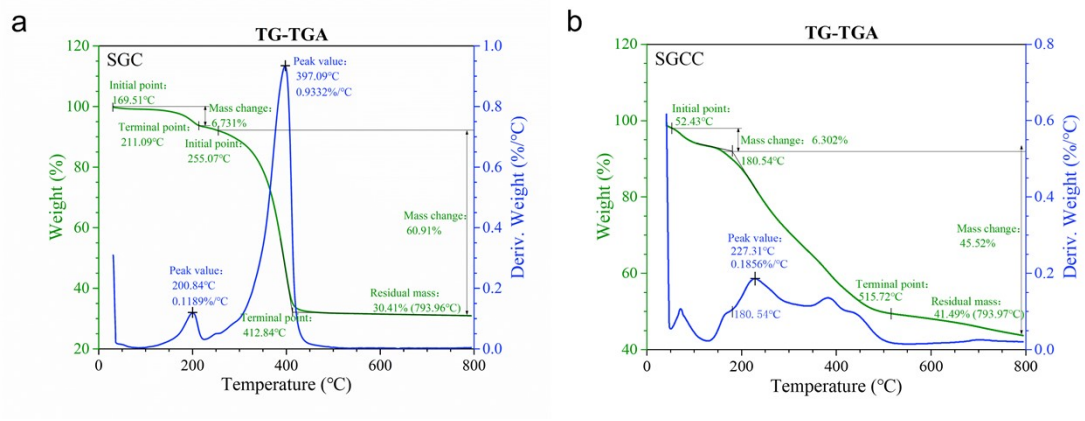

Fig. S12. The TG curves of (a) SGC and (b) SGCC.

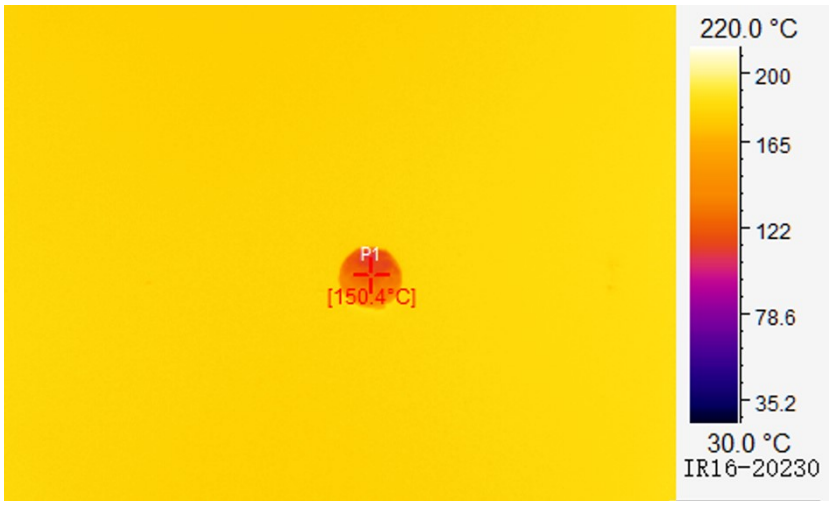

Fig. S13. Thermal image of SGCC after 30 minutes of continuous heating.

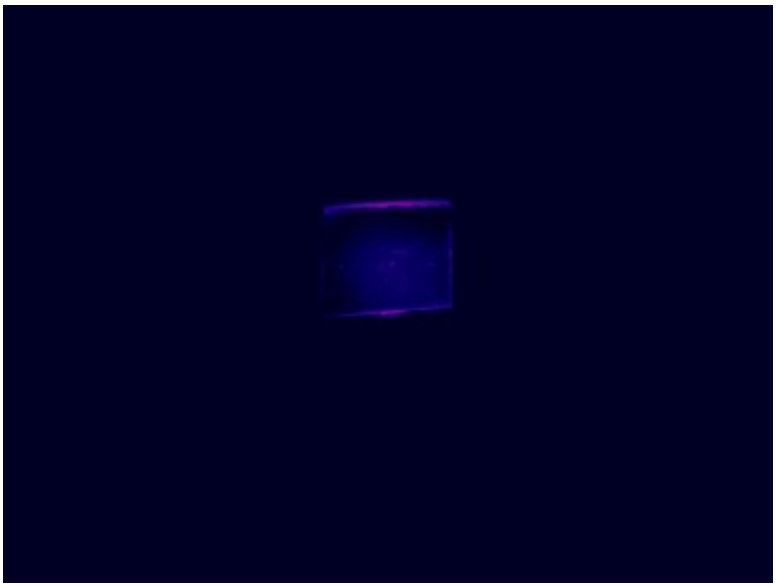

Fig. S14. Infrared image of SGCC/ITO during the cooling process before disappearing from the field of view.

Table. S1 Anisotropic Thermal Conductivity Testing of SGCC.

	Thermal conductivity (in-plane) (W/m·k)	Thermal conductivity (through-plane) (W/m·k)
First Test	0.033455	0.028476
Second Test	0.033548	0.028719
Third Test	0.033754	0.028225
Average	0.033585667	0.028473333

Table. S2 Comparison of thermal management capabilities in terms of applications.

No.	Material	Applicable temperature	Cooling effect (Δ T)	Ref
1	H-rGO/PVA-3	60	4.1	[14]
2	CuS@rGO composite aerogels	120	89.89	[15]
		120	93.14	
3	ATO/rGO aerogels	80	50	[16]
4	PI/graphene/Fe3O4 hybrid aerogel film	90	＜42.5	[17]
5	CCB-SCP/Chitosan	200	41.8	[18]
		190	46	
6	MXene/reduced graphene oxide hybrid aerogel composites	50	13	[19]
7	MXene/rGO composite aerogel	50	19	[20]
8	polyvinyl alcohol/carboxylated carbon nanotubes/graphene hybrid aerogels	65	18.8	[21]
9	PEG/PC10	100	43	[22]
	PEG/PC15	100	41.1	
	PEG/PC20	100	37.6	
10	paraffin wax/carbon nanotube sponge composites	65	24	[23]
11	3D multi-wall carbon	120	44	[24]

	nanotubes/graphene/silicone rubber elastomer			
	GA/SR	120	61.5	
12	anisotropic cellulose nanofiber/chitosan aerogel (5mm)	200	114.2	[25]
13	nanocellulose/chitosan aerogels (5mm)	200	136	[26]
this work	SGCC (2mm)	200	85.1	\
	SGCC/ITO	200	140.08	

Table. S3 Comparison of thermal conductivity.

No.	Material	Thermal conductivity ($W \cdot m^{-1} \cdot K^{-1}$)	Ref
1	H-rGO/PVA-3	0.88	[14]
	H-rGO/PVA-4	6.15	
	H-rGO/PVA-5	5.9	
2	rGO/PVA	2.02	[27]
3	CCB-SCP/Chitosan	0.018	[18]
4	MXene/rGO composite aerogel	0.026	[20]
5	polyvinyl alcohol/carboxylated carbon nanotubes/graphene hybrid aerogels	0.64	[21]
6	TSC-10	0.51	[28]
	TLC-10	0.45	
	TSW-10	0.5	
7	PEG/PC10	0.363	[21]
	PEG/PC15	0.486	

	PEG/PC20	0.568	
8	paraffin wax/carbon nanotube sponge composites	1.85	[23]
9	3D multi-wall carbon nanotubes/graphene/silicone rubber elastomer	1.3	[24]
10	SC/50M@PCM	0.316	[29]
11	the silylated chitosan aerogel	0.0304	[30]
12	anisotropic cellulose nanofiber/chitosan aerogel	0.028 (in rational direction), 0.036 (in the axial direction)	[25]
13	nanocellulose/chitosan aerogels	0.027 (in the radial direction), 0.033 (in the axial direction)	[25]
this work	SGCC	0.028	\

References:

[1] Nie J, Lu W, Ma J, et al. Orientation in multi-layer chitosan hydrogel: morphology, mechanism and design principle[J]. Scientific reports, 2015, 5(1): 1-7.

[1] Jorgensen W L, Maxwell D S, Tirado-Rives J. Development and testing of the OPLS all-atom force field on conformational energetics and properties of organic liquids [J]. Journal of the American Chemical Society, 1996, 118 (45): 11225-11236.

[2] Hendrik Heinz R. A. Vaia B. L. Farmer R. R. Naik. Accurate Simulation of Surfaces and Interfaces of Face-Centered Cubic Metals Using 12−6 and 9−6 Lennard-Jones Potentials[J]. J. Phys. Chem. C 2008, 112, 17281–17290.

[3] Spoel D V D, Lindahl E, Hess B, et al. GROMACS: fast, flexible, and free[J]. Journal of Computational Chemistry, 2005, 26(16): 1701-1718.

[4] Abraham, et al. GROMACS: high performance molecular simulations through multi-level parallelism from laptops to supercomputers, SoftwareX. 1-2 (2015) 19–25.

[5] H.J.C. Berendsen, D. van der Spoel, R. van Drunen,GROMACS: A message-passing parallel molecular dynamics implementation,Comp. Phys. Comm., 91 (1995) 43-56.

[6] Van Gunsteren, W. F.; Berendsen, H., A leap-frog algorithm for stochastic

dynamics. Mol. Simul. 1988, 1 (3), 173-185
[7] Hess, B.; Bekker, H.; Berendsen, H. J.; Fraaije, J. G., LINCS: a linear constraint solver for molecular simulations[J]. J. Comput. Chem. 1997, 18 (12), 1463-1472.
[8] Darden T, York D, Pedersen L. Particle Mesh Ewald: An Nlog (N) Method for Ewald Sums in Large Systems [J]. The Journal of Chemical Physics, 1993,98(12):10089-10092.
[9] Kresse, G. & Hafner, J. Ab initio molecular dynamics for liquid metals. Phys. Rev. B 47, 558–561 (1993).
[10] Kresse, G. & Furthmüller, J. Efficient iterative schemes for ab initio total-energy calculations using a plane-wave basis set. Phys. Rev. B 54, 11169–11186 (1996).
[11] Perdew, J. P., Burke, K. & Ernzerhof, M. Generalized Gradient Approximation Made Simple. Phys. Rev. Lett. 77, 3865–3868 (1996).
[12] Blöchl, P. E. Projector augmented-wave method. Phys. Rev. B 50, 17953–17979 (1994).
[13] Grimme, S., Ehrlich, S. & Goerigk, L. Effect of the damping function in dispersion corrected density functional theory. J. Comput. Chem. 32, 1456–1465 (2011).
[14] Huo J, Zhang G, Yuan X, et al. Electrospraying graphene nanosheets on polyvinyl alcohol nanofibers for efficient thermal management materials[J]. ACS Applied Nano Materials, 2023, 6(7): 6241-6246.
[15] Wu Y, Zhao Y, Zhou M, et al. Ultrabroad microwave absorption ability and infrared stealth property of nano-micro CuS@ rGO lightweight aerogels[J]. Nano-micro letters, 2022, 14(1): 171.
[16] Li J, Xu Z, Li T, et al. Multifunctional antimony tin oxide/reduced graphene oxide aerogels with wideband microwave absorption and low infrared emissivity[J]. Composites Part B: Engineering, 2022, 231: 109565.
[17] Shi T, Zheng Z, Liu H, et al. Configuration of multifunctional polyimide/graphene/Fe3O4 hybrid aerogel-based phase-change composite films for electromagnetic and infrared bi-stealth[J]. Nanomaterials, 2021, 11(11): 3038.
[18] Hu J, Hu Y, Yang J, et al. Nano-assembled modified graphene composites based on rapid microwave fabrication for thermal management[J]. Chemical Engineering Journal, 2023, 476: 146670.
[19] Li B X, Luo Z, Yang W G, et al. Adaptive and adjustable MXene/reduced graphene oxide hybrid aerogel composites integrated with phase-change material and thermochromic coating for synchronous visible/infrared camouflages[J]. ACS nano, 2023, 17(7): 6875-6885.
[20] Yu C, Lin D, Guo J, et al. Ultralight Three‐Layer Gradient‐Structured MXene/Reduced Graphene Oxide Composite Aerogels with Broadband Microwave Absorption and Dynamic Infrared Camouflage[J]. Small, 2024: 2401755.
[21] He F, Hong W, Liu Z, et al. Shape-stabilized phase change materials based on polyvinyl alcohol/carboxylated carbon nanotubes/graphene hybrid aerogels for

efficient solar-thermal conversion and thermal camouflage[J]. Solar Energy Materials and Solar Cells, 2024, 274: 112973.
[22] Luo W, Luo L, Ma Y, et al. Highly thermal conductive phase change materials enabled by CNTs-modified PVA aerogel for solar energy storage and thermal management of electronic components[J]. Journal of Energy Storage, 2024, 88: 111583.
[23] Lu X, Zheng Y, Yang J, et al. Multifunctional paraffin wax/carbon nanotube sponge composites with simultaneous high-efficient thermal management and electromagnetic interference shielding efficiencies for electronic devices[J]. Composites Part B: Engineering, 2020, 199: 108308.
[24] Liu D, Kong Q Q, Jia H, et al. Dual-functional 3D multi-wall carbon nanotubes/graphene/silicone rubber elastomer: Thermal management and electromagnetic interference shielding[J]. Carbon, 2021, 183: 216-224.
[25] Zhang M, Jiang S, Han F, et al. Anisotropic cellulose nanofiber/chitosan aerogel with thermal management and oil absorption properties[J]. Carbohydrate polymers, 2021, 264: 118033.
[26] Chaudary A, Patoary M K, Zhang M, et al. Structurally integrated thermal management of isotropic and directionally ice-templated nanocellulose/chitosan aerogels[J]. Cellulose, 2022, 29(15): 8265-8282.
[27] Alam F E, Dai W, Yang M, et al. In situ formation of a cellular graphene framework in thermoplastic composites leading to superior thermal conductivity[J]. Journal of materials chemistry A, 2017, 5(13): 6164-6169.
[28] Shin B, Mondal S, Lee M, et al. Flexible thermoplastic polyurethane-carbon nanotube composites for electromagnetic interference shielding and thermal management[J]. Chemical Engineering Journal, 2021, 418: 129282.
[29] Fu L, Wu Z, Wu K, et al. A thermally induced flexible composite phase change material with boron nitride nanosheets/carbon nanotubes modified skeleton for battery thermal management[J]. Applied Energy, 2024, 373: 123899.
[30] Xiao W, Wang P, Song X, et al. Facile fabrication of anisotropic chitosan aerogel with hydrophobicity and thermal superinsulation for advanced thermal management[J]. ACS Sustainable Chemistry & Engineering, 2021, 9(28): 9348-9357.